Structural Eng./Earthquake Eng. Vol. 12, No. 2, 53s—65s, July 1995
Japan Society of Civil Engineers (J. Struct. Mech. Earthquake Eng. No. 519/ I—32)

A FATIGUE CRACK GROWTH PREDICTION MODEL WITH LOAD INTERACTION EFFECTS USING CRACK CLOSURE CONCEPT

Xiaohua CHENG[1] and Kentaro YAMADA[2]

[1]Member of JSCE, Dr. of Eng., Bridge Division, Public Works Research Institute, Ministry of Construction, (Asahi 1, Tsukuba 305, Japan, Former Graduate Student, Nagoya University)
[2]Member of JSCE, Ph. D., Professor, Dept., of Civil Eng., Nagoya University (Furo-cho 1, Chikusa-ku, Nagoya 464-01, Japan)

Crack closure phenomenon is observed in center-cracked tension (CCT) specimens of structural steel JIS SM520B. The remaining plastic deformation in the wake of an advancing crack causing crack closure is a significant factor of the load interaction effects on fatigue crack growth rates. A prediction model based on crack closure concept is used to compute fatigue crack opening stress and consequently effective stress intensity factor range, ΔK_{eff}, and correlate it with the measured fatigue crack growth rates. The analytical results are compared with test results under overload conditions. Fatigue crack propagation lives are computed under various load sequences to investigate the load interaction effects.

Key Words : *crack closure, opening stress, effective stress range, fatigue crack growth, load interaction effect*

1. INTRODUCTION

Miner's rule and Paris' equation are normally used to predict fatigue crack propagation life under variable amplitude (VA) loading conditions. Although they do not consider any load sequence or load interaction effects, analytical results often correspond well with test results when a high stress ratio is applied, or a high tensile residual stress exists. It may be because the fatigue crack always opens. This case is called crack closure-free condition[1]. When a low stress ratio condition exists or applied stress ranges are low, such as in case of highway bridges, the fatigue crack growth behavior under a random load sequence are not fully understood. Analytical results under various spectrum loadings indicate the needs of further investigation on the load interaction effects in long life region[2].

The load interaction effect is significant when an overload is applied before stress cycles of lower level or when an underload is applied before stress cycles of higher level[3),11]. The degree of the effects depends on magnitude, number, stage of the application of overload or underload, stress levels after overload or underload and so on[4),5),6]. For example, the fatigue test results by Abtahi *et al.*[7], Albrecht & Yamada[8] and Melhem & Klippstein *et al.*[9] indicated that periodic overloads or long-tail spectrum load conditions in high stress range region seem to affect fatigue crack propagation life, especially in long life region. The effect depends on the overload period or the block size of spectrum loadings.

In order to predict the fatigue crack growth behavior under a complex load sequence, some analytical models have been developed. For example, Wheeler's model[10] and Elber's model[11] are the relatively simple ones to explain the load interaction effect after overloads. Since crack closure under cyclic tensile loading was first observed by Elber[11], the crack closure concept is widely used to explain fatigue problems. The plastic deformation generated ahead of crack tip and remained behind the crack tip is taken into account to develop fatigue crack growth prediction models under constant and variable amplitude loadings. Newman[12], Zhang[5] and Chermahini[13] *et al.* carried out analyses on fatigue crack closure and fatigue crack growth by using 2D or 3D elasto-plastic Finite Element Method. The FEM analysis normally requires a large amount

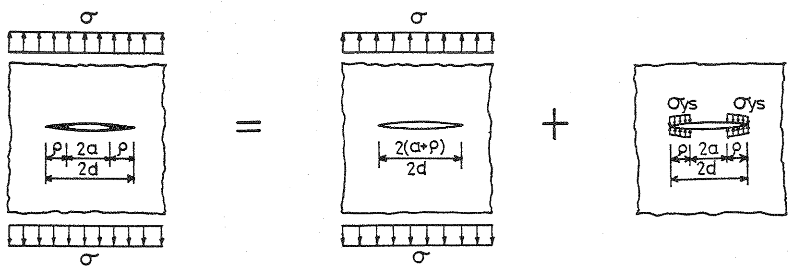

$$K = K_{\sigma} + K_{\sigma_{ys}}$$

$$COD = (COD)_{\sigma} + (COD)_{\sigma_{ys}}$$

Fig. 1 Superposition of two elastic solutions of fictitious crack

of computation, and it is not feasible to compute a wide range of fatigue crack growth. Simplified numerical analyses based on Dugdale's plastic zone model and Elber's crack closure concept are also carried out by Newman[14)], Koning[15)] and Wang & Blom[16)] *et al.*, which still keep a certain accuracy in the analysis.

In the present study, a planar prediction model of discretized plastic bar elements based on crack closure concept is applied in order to predict fatigue crack growth due to effective stress intensity factor range, ΔK_{eff}. The model is similar to Newman's model, but the constraint factor (α) of plastic deformation is proposed to vary both with the plate thickness and the process of fatigue crack growth. The ultimate goal of the present study is to obtain a quantitative prediction of fatigue crack growth by a relatively simple method for a complex loading condition. The analytical results are compared with fatigue crack growth rate measurements and fatigue crack closure test results on center-cracked tension (CCT) specimens of structural steel JIS SM520B. A part of the test results has been published elsewhere[4)]. The effects of various parameters, such as constraint factor and stress ratio, on opening stress are investigated. The effective stress intensity factor range, ΔK_{eff}, is correlated with the fatigue crack growth rates. Fatigue crack propagation lives under various load conditions are also predicted.

2. PREDICTION MODEL

(1) Crack closure, contact stress and opening stress

Crack closure phenomenon was observed in some metallic materials upon unloading under constant amplitude (CA) loadings[6),11)]. It is also called plasticity-induced closure[17)]. Both the contact stress on the crack surfaces and the residual stress built up in the plastic zone at crack tip result from the same action of the surrounding elastic material on the plastically deformed material under unloading. The subsequent load cycle can cause crack growth only when the contact stresses along the crack surfaces are overcome, so that the crack fully opens. The nominal stress to open crack fully is called crack opening stress, σ_{op}. The fatigue crack growth is attributed to the effective stress intensity factor range, ΔK_{eff}, after crack fully opens.

$$\Delta K_{eff} = K_{max} - K_{op} \qquad (1)$$

where K_{max} and K_{op} are the stress intensity factors corresponding to the maximum stress and the opening stress, respectively.

(2) Assumptions

In the present study, the following assumptions are made to make the model consistent with the physical behavior in cracked body in fatigue condition and to keep it still simple.

(a) At crack tip the plastic zone size is assumed to be equivalent to the Dugdale's plastic zone size[18)]. Adopting Dugdale's plastic zone model, all the plastic deformations in the plastic zone are assumed to be concentrated in a very narrow layer of material along the crack line. The plastic deformations form a tapered narrow strip from crack tip to a fine point, as shown in the dark areas in **Fig.1**.

(b) Cyclic stress-strain behavior of the material is assumed to be elastic-perfectly plastic[22)]. The basic yield stress, σ_s, is obtained from uniaxial tensile test of the material.

(c) The constraint effect on the plastic deformation in the plate thickness direction is accounted for by the constraint factor α. The equivalent tensile yield stress is defined as $\sigma_{ys}=\alpha\cdot\sigma_s$. While the constraint effect on the reverse plastic deformation under compressive stress is neglected in the computation, namely $\sigma_{ys}=-\sigma_s$, because (i)

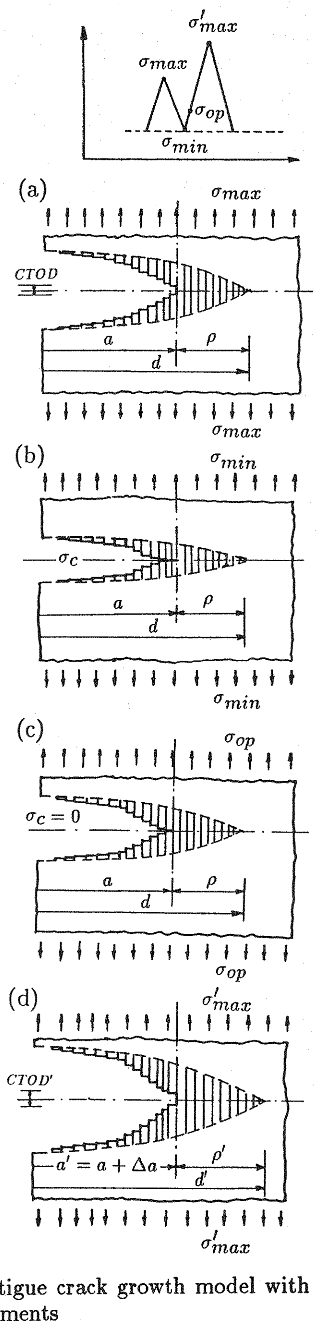

Fig. 2 Fatigue crack growth model with discretized elements

the compressive plastic zone is small compared with the tensile one, so that it locates just at the blunting crack front, and (ii) on the crack surfaces behind the crack tip the free deformation is dominant.

(d) The plastic deformation on crack surface or ahead of crack tip is permanent, unless stress exceeds the equivalent yield stress σ_{ys} (*i.e.*, $\alpha \cdot \sigma_s$ or $-\sigma_s$).

(e) Crack extension is assumed to occur, when the maximum load σ_{max} is applied. Fatigue crack extends step by step with a given crack length increment or a given number of load cycles.

(3) Analytical approach

The plastic zone near the physical crack tip is shown in **Fig.1**, based on Dugdale's plastic zone model. If the boundary of the elastic and the plastic zones is assumed as fictitious crack surfaces, the elasto-plastic problem around the physical crack can be simplified to an elastic problem on the fictitious crack, as shown in **Fig.1**. Two elastic solutions of fictitious crack under external load and yield stress distributed along the fictitious crack surfaces in the plastic zone can be superposed. Small scale yielding condition is required, that is, the plastic zone size at crack tip is small compared with the crack size.

The Dugdale's plastic zone at physical crack tip is divided into several bar elements, of which lengths (L_i) are equal to the opening displacements (v_i or COD) of the fictitious crack. The bar element length also corresponds to the permanent plastic deformations of the material along the crack line ahead of the crack tip. Upon unloading, however, when the residual stresses on the elements in the plastic zone or the contact stresses on the elements in the crack wake are over the compressive yield stress, the element length decreases due to reverse plastic deformation. When element length increases due to the extended crack length or higher peak load, the element length at the same position should be changed to the larger value. Otherwise the element lengths are kept at the permanent values.

The crack opening, crack closure and crack growth behavior are schematically demonstrated in **Fig.2**. One load cycle is from the maximum peak to the next maximum peak via the minimum valley.

(a) At the σ_{max}, the crack fully opens. Since there is no singularity at the fictitious crack tip, Dugdale's plastic zone size, ρ_{Dug}, can be obtained by the relation of $K = K_{\sigma_{max}} + K_{\sigma_{ys}} = 0$ at fictitious crack tip, as shown in **Eq.2** for a CCT specimen under remote loading[14]:

$$\rho_{Dug} = a\left\{\frac{2W}{\pi a}\sin^{-1}\left[\sin\left(\frac{\pi a}{2W}\right)\sec\left(\frac{\pi\sigma_{max}}{2\sigma_{ys}}\right)\right] - 1\right\} \tag{2}$$

where a is the half crack length, $2W$ is the plate width of specimen, and σ_{ys} is the equivalent tensile yield stress. It is worth mentioning that the specimen should be in the state of small scale yielding, or under a load of $\sigma \leq 0.6\sigma_s$.

In Dugdale's plastic zone, the plastically deformed element length, L_i, is equal to the opening displacement of fictitious crack, v_i.

$$L_i = v_i = \sigma_{max} \cdot f(x_i) - \sum_{\rho} \sigma_{ys} \cdot g(x_i, x_j) \quad (3)$$

where $f(x_i)$ and $g(x_i, x_j)$ are the factors related to geometry of specimen. $f(x_i)$ is the fictitious crack opening displacement at the element i due to unit remote load, while $g(x_i, x_j)$ is the fictitious crack opening displacement at element i due to the uniformly distributed unit load at element j. Both factors are with the plate width correction[14),15)]. Under σ_{max}, crack tip blunting also occurs, shown as CTOD. The degree of the crack tip blunting depends on the maximum load magnitude.

(b) When unloading, since there are permanent plastic elongations previously remaining on the physical crack surfaces, the crack closure occurs in the wake of crack over some distance. If L_i is greater than the present v_i under σ_{min}, the crack surfaces contact at element i. On the contrary, if L_i is less than v_i, the crack surfaces are untouched at element i. When the crack surfaces contact, the compatibility equation of fictitious crack opening displacement is:

$$v_i = L_i = \sigma_{min} \cdot f(x_i) - \sum_{a+\rho} \sigma_j \cdot g(x_i, x_j) \quad (4)$$

where the stress σ_j is contact stress, σ_c, for $0 < x_i < a$ or residual stress, σ_{re}, for $a < x_i < a + \rho$ upon unloading. The stress σ_i at element i can be calculated by iteration as follows.

$$\sigma_i = [\sigma_{min} \cdot f(x_i) - L_i - \sum_{j \neq i}^{a+\rho} \sigma_j \cdot g(x_i, x_j)]/g(x_i, x_i) \quad (5)$$

During the iteration, the restraint conditions are added in each iteration step. They are:

for $x_i > a$, *i.e.* in plastic zone,
  if $\sigma_i > \sigma_{ys}$, then $\sigma_i = \sigma_{ys}$
  if $\sigma_i < -\sigma_s$, then $\sigma_i = -\sigma_s$
for $x_i < a$, *i.e.* on the crack surfaces,
  if $\sigma_i > 0$, then $\sigma_i = 0$
  if $\sigma_i < -\sigma_s$, then $\sigma_i = -\sigma_s$

The iteration is continued until the difference of the stresses in the two adjacent steps is less than 0.1% of the yield stress σ_s.

(c) In order to make crack open fully, at least the load increment $\sigma_{op} - \sigma_{min}$ should be applied on σ_{min} to overcome the contact stresses. The opening stress σ_{op} is determined by the displacement method, as follows.

The crack opening displacement at element i on the physical crack surface due to load increment $(\sigma_{op} - \sigma_{min})$ is set equal to the displacement due to the contact stresses. In this case the contact stress at element i is overcome, but the relative displacement between the two surfaces of physical crack is zero. It is when the crack surfaces at element i start to separate. The maximum value of $(\sigma_{op} - \sigma_{min})_i$ for all elements on the physical crack surfaces gives the opening stress for crack fully opening. For element i, that is:

$$(\sigma_{op})_i = \sigma_{min} - \sum_{a} \sigma_j \cdot g'(x_i, x_j)/f'(x_i) \quad (6)$$

where σ_j is the contact stress in the wake of crack upon unloading to σ_{min}, and $f'(x_i)$ and $g'(x_i, x_j)$ correspond to the physical crack length a.

(d) Under reloading, the new plastic deformation at crack tip may occur only after the crack fully opens. With load increasing, crack opens again. New plastic zone at crack tip is formed by the new maximum load, σ'_{max}. The fatigue crack extends a certain amount, for example one element width, upon the effective stress range, $\Delta\sigma_{eff} (=\sigma_{max} - \sigma_{op})$, and the plastically deformed element at the previous crack tip remains in the wake of the advancing crack.

(e) With the same process continuing, the fatigue crack propagates under cyclic loading. Because the plastic deformations remaining on the crack surfaces can "memorize" the previous load sequence effect, the present model based on the crack closure concept can consider the load interaction effect on the fatigue crack growth rates.

3. ANALYSIS UNDER CONSTANT AMPLITUDE LOADING

(1) COD and stresses at crack tip

In order to observe the crack opening displacement (COD) at σ_{max}, plastic deformation remaining on the crack surface and contact stress at σ_{min}, the analysis is carried out with the centrally cracked plate of 10 mm thick and 130 mm wide under CA loading. The material is structural steel SM520B with basic yield stress σ_s = 401.8 MPa[4)]. The analytical results are shown in **Fig.3**.

Fig.3(a) shows one fourth of the physical crack and fictitious crack. The dotted line expresses the fictitious crack surface, which is the boundary of elastic and plastic materials. The shaded regions show the plastic deformation ahead of the

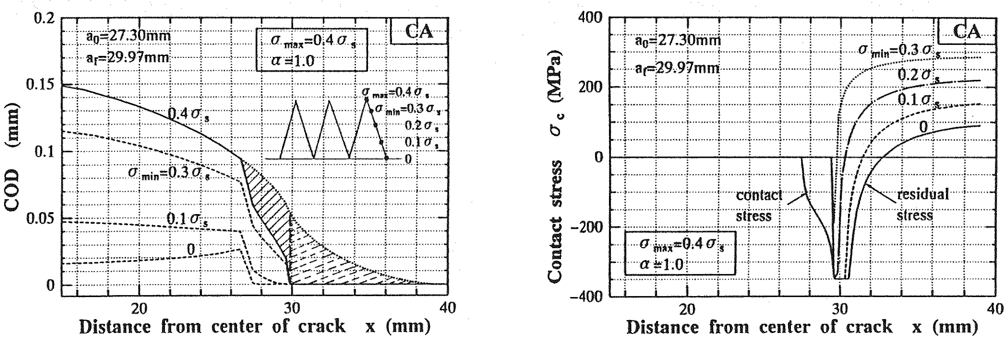

(a) at the maximum stress σ_{max} (b) at the minimum stress σ_{min}

Fig. 3 COD, residual stress and contact stress

crack tip and the residual plastic deformation behind the crack tip. The solid line is the physical crack surface at $\sigma_{max} = 0.4\sigma_s$. From the profile of COD, it is noted that without residual plastic deformation remaining on the crack surface, the crack tip opening displacement (CTOD) is equal to the plastic elongation at crack front. This is the case of sharp crack-like saw-cut. For the fatigue crack, the physical CTOD is smaller due to the residual plastic deformation remaining on the crack surface. Consequently, at unloading the crack closes near the crack tip. The dashed lines show the physical crack surfaces at different unloading levels. The lower unloading level causes the wider crack closure near the crack tip, and therefore, the more contact stress is observed.

The contact stress in the wake of crack and residual stress ahead of crack tip are shown in **Fig.3(b)**. At unloading the elastic material around the crack tip plastic zone squeezes the plastically deformed material. Near the crack tip the residual stress is lower because of the more plastic deformation formed. If unloading is low enough, the compressive yielding occurs near the crack tip, and the contact stress on the crack surfaces becomes larger.

(2) Effect of constraint factor

The constraint factor α is introduced to account for the constraint effect in plate thickness direction on the plastic deformation at crack tip. It varies with the ratio of plate thickness (t) to plastic zone size (ρ) near crack tip, t/ρ, when fatigue crack propagates. When $t/\rho \leq 1$, plane stress condition can be assumed and $\alpha \approx 1.0$. At the other extreme, plane strain condition can be assumed near the crack tip, and $\alpha \approx 1.68$ when $t/\rho \geq 18$[4),22)]. In general case the state of stress at crack tip is between the two stress states where $1 \leq \alpha \leq 1.68$. The linear interpolation method is proposed in the present study to approximately determine the value of α[23)], that is,

$$\alpha = 1.0 + \frac{0.68}{17} \cdot (t/\rho - 1.0) \qquad (7)$$

Fatigue crack propagation life of CCT specimens of 10 mm thick is computed with both the fixed value of α=1.68 and values given by **Eq.(7)** during crack growth under CA loading. They are plotted along with the test results (**Table 1** and **Ref.4**), as shown in **Fig.4(a)**. In this case the plane strain state can be assumed during the whole crack growth period. Only in the late stage of the fatigue crack propagation the effect of α becomes larger, because the larger plastic zone size causes less constraint effect. The effect is larger for higher stress ratio and higher stress range.

Opening stresses with different constraint factors α are calculated for an initial crack length, a_0 = 10 mm. The results are shown in **Fig.4(b)**. The higher value of α or thicker plate causes lower opening stress due to the more constraint effect on the plastic deformation.

(3) Effect of stress ratio

The opening stresses are also calculated for different stress ratios. The analytical results are shown in **Fig.5(a)**, where the maximum stress is kept at $\sigma_{max} = 0.4\sigma_s$ and the stress ratio R is changed from -1 to 0.9. Three constraint factors are also used as α=1.0, 1.25 and 1.68. The computed σ_{op} is normalized by σ_{max}. The higher stress ratio or the higher minimum stress σ_{min} causes higher opening stress, which is due to the higher unload level. It is also observed that the higher α causes the lower opening stress at the same stress ratio R. The difference in σ_{op} at

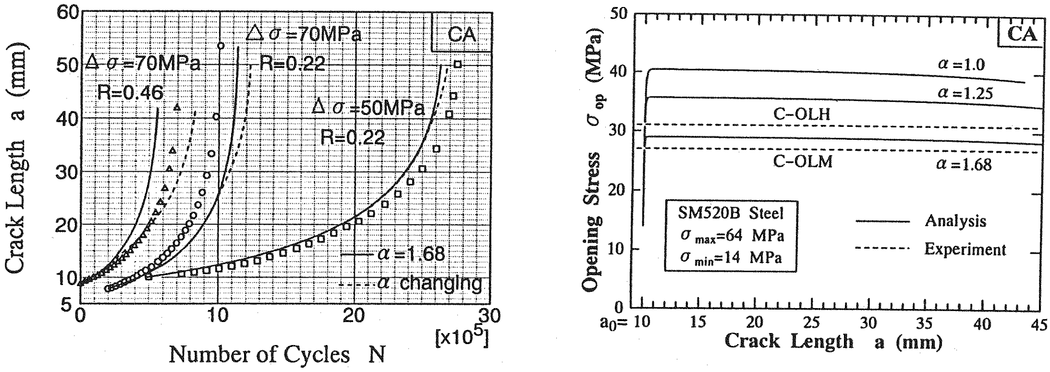

(a) Computed fatigue crack propagation life (b) Opening stress

Fig. 4 Analysis with various constraint factors under CA loading

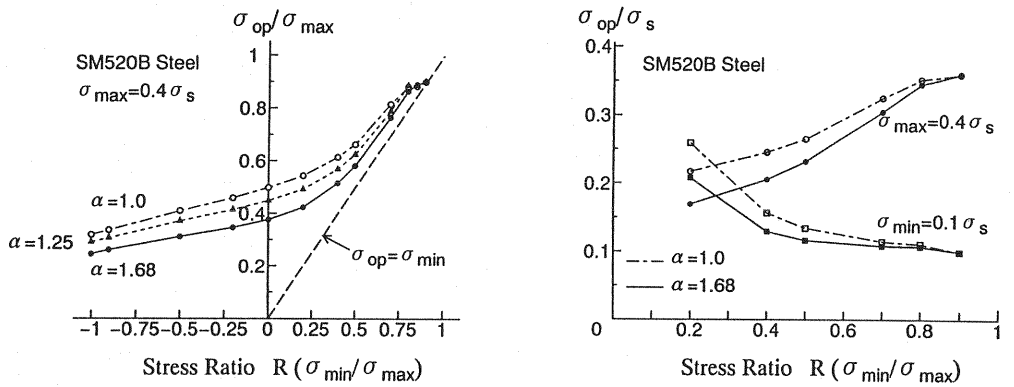

(a) for the constant maximum stress σ_{max} (b) for the constant minimum stress σ_{min}

Fig. 5 Opening stress at various stress ratios

$R = 0$ is about 30%, when plane strain (α=1.68) and plane stress (α=1.0) conditions are assumed. At $R < 0$, the change in σ_{op} is little. While at $R > 0$, σ_{op} increases rapidly as R increases. When $R \geq 0.7$, the opening stress σ_{op} becomes independent of R and α. In this case, crack always opens and the value of σ_{op} coincides with σ_{min}.

When σ_{min} is constant, such as $\sigma_{min} = 0.1\sigma_s$, the lower stress ratio or the higher σ_{max} causes higher σ_{op}, as shown in **Fig.5(b)**. The more plastic deformation due to the higher load level attributes to it. It is worth mentioning that at the same stress ratio, opening stress depends both on load level σ_{max} and unload level σ_{min}.

(4) Comparison with test results

In order to re-examine the crack closure phenomenon in structural steel and to verify the present analytical model, the fatigue crack closure test is carried out on CCT specimens of JIS SM520B steel[4]. The strain gage arrangement is shown in **Fig.6(a)**. Crack opening stress σ_{op} is determined graphically by taking the transient point of stage 2 and 3, as shown in **Fig.6(b)**. The test specimens is listed in **Table 1**.

The measured σ_{op} before overload, which corresponds to CA loading condition, is about 31 MPa for specimen C-OLH and 27 MPa for C-OLM. The average value of the two, about 29 MPa, is in a good agreement with the analytical result, as shown in **Fig.4(b)** in plane strain state.

The opening stresses are also computed for the other specimens tested at stress ratios of R=0.22 and 0.46 and stress ranges of $\Delta\sigma$=70 and 50 MPa under CA loading[4]. Consequently, the effective stress intensity factor ranges, ΔK_{eff}, are computed. The fatigue crack growth rates are replotted by correlating with ΔK_{eff}, as shown in **Fig.7**. The fatigue crack growth rates are also plotted against ΔK. For comparison, the previous test results, from National Research Institute for Metals (NRIM)[19] and Nagoya University

Table 1 Specimens for crack closure test

Specimen No.	$\Delta\sigma$ (MPa)	σ_{max} (MPa)	σ_{min} (MPa)	R ($\sigma_{min}/\sigma_{max}$)	R_{OL} (σ_{OL}/σ_{max})	σ_{OL} (MPa)
C-CA	50	64	14	0.22	-	-
C-OLH	50	64	14	0.22	2.0	128.0
C-OLM	50	64	14	0.22	1.7	108.8

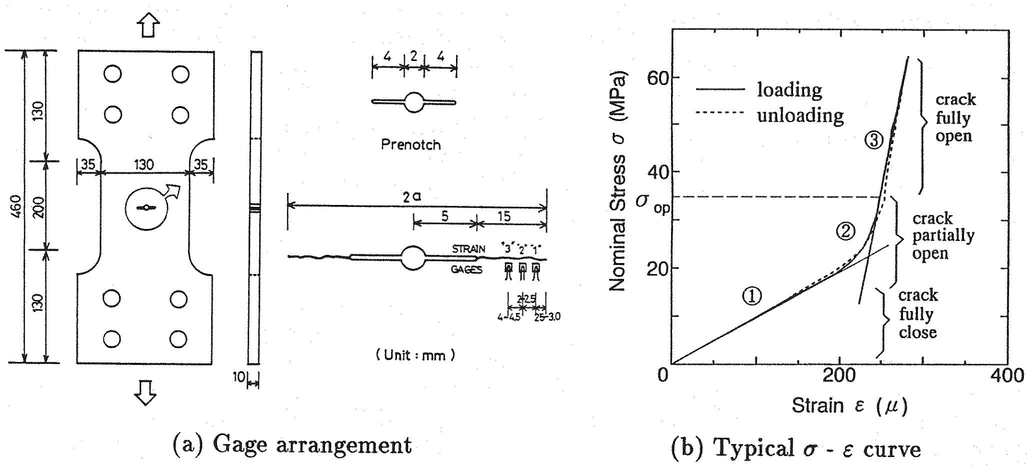

Fig. 6 Fatigue crack closure test

(NUCE)[20], as well as the mean design curve of Japanese Society of Steel Construction (JSSC)[21] are plotted. In the present test fatigue crack growth rates are almost on the same curve for various stress ratios. The difference between the two sets of the data in **Fig.7** lies on the consideration of opening stress, or saying load interaction effect. Without considering opening stress, the data of $da/dN-\Delta K$ are slightly higher than those of base material from NUCE. With considering opening stress, the data of $da/dN-\Delta K_{eff}$ are higher than the mean values of welded joints from NRIM and the mean design curve of JSSC, both of which are set based on the test data with weld residual stress. Since the linear part of fatigue crack growth rates is considered in the present experimental and analytical study, the empirical equations of da/dN for the present test data can be expressed as:

without considering opening stress, that is, traditional Paris' Equation,

$$\frac{da}{dN} = C(\Delta K)^m, m = 3.371, C = 2.382 \times 10^{-12} \quad (8)$$

with considering opening stress,

$$\frac{da}{dN} = C(\Delta K_{eff})^m, m = 3.257, C = 9.321 \times 10^{-12} \quad (9)$$

where the material constants m and C are determined by the least square method. The effective stress intensity factor range $\Delta K_{eff}=\Delta\sigma_{eff}\cdot F(a)\cdot\sqrt{\pi a}$ in which $\Delta\sigma_{eff} = \sigma_{max} - \sigma_{op}$ and $F(a)$ is a correction factor. **Eq.(9)** is used in the fatigue crack propagation life prediction with considering the effect of σ_{op}.

4. ANALYSIS UNDER OVERLOAD CONDITIONS

(1) Crack growth process

Using the prediction model based on the crack closure concept, fatigue crack growth process is simulated under overload condition. The analysis is carried out from a = 18 mm. Fatigue crack extension in one step is assumed as the element width at crack front, which is 1/40 of the plastic zone size, because the computed opening stress σ_{op} converges when element width at crack tip is in this order. At the overload application, fatigue crack extends the amount corresponding to one overload cycle in accordance with **Eq.(9)**. With fatigue crack growth the results of COD and contact stress are shown in **Fig.8**. Fictitious crack surface at applied σ_{max} is plotted by dashed line. The real COD is plotted by solid line. The elastic solution of physical COD is plotted by dotted

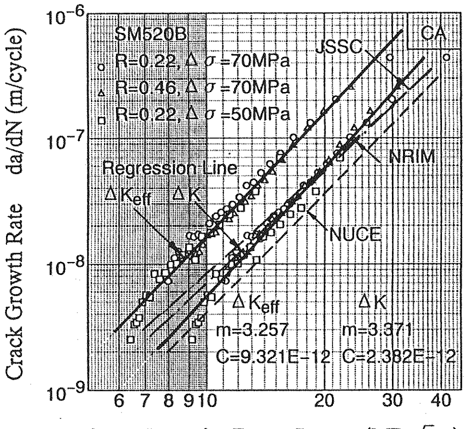

Fig. 7 Crack growth rates under CA loading

line. In the region between dashed line and solid line, there are plastic deformations.

Before overload application, the real CTOD becomes smaller due to the residual plastic deformations remaining on the crack surfaces, as shown in **Fig.8(a)**

When an overload is applied with the overload ratio $R_{OL}=\sigma_{OL}/\sigma_{max}=1.7$, the crack tip is blunted, as shown in **Fig.8(b)**. The real CTOD and plastic zone size are larger than those due to σ_{max} of CA loading. When unloading to σ_{min}, the surrounding elastic material squeezes the larger plastic deformation, and near the crack tip more compressive yielding occurs.

After the overload application, the plastic zone size, ρ, due to the normal σ_{max} is smaller than the overload plastic zone size, ρ_{OL}. The plastic deformation ahead of crack tip due to the σ_{max} is also smaller than that generated by overload. As shown in **Fig.8(c)**, the tapered region ahead of crack tip expresses the residual overload plastic zone and plastic deformations. The fictitious COD is calculated by the superposition of the fictitious CODs under the remote σ_{max} and the uniformly distributed σ_{ys} in the residual overload plastic zone, when the crack extends through the overload plastic zone after overload. Noting that, in the residual overload plastic zone, fictitious crack surface is selected as the larger value between the computed superposition value and the previous residual plastic deformation. At σ_{min}, the element length changes when the compressive stress causes reverse plastic yielding.

When the crack grows, the residual deformations remaining on the crack surfaces gradually form a ridge, as shown in **Fig.8(d)** and **(e)**, which is the memory of the overload effect. The height and width of the ridge depend on the magnitude of the overload and the overload plastic zone size. This ridge increases contact stress at unloading and consequently σ_{op} locally increases.

As the crack extends through the overload plastic zone, the leading edge of plastic zone moves when the fictitious crack length $(a+\rho)$ due to σ_{max} is larger than $(a_{OL}+\rho_{OL})$ due to overload. The overload effect diminishes when the residual plastic deformations near crack tip gradually recover to the same situation as before overload, as shown in **Fig.8(f)**. At this stage, the ridge region is far away from the crack tip, and has little effect on the contact stress at unloading.

The contact stresses under σ_{min} are also obtained for the corresponding crack length. It can be seen in **Fig.8(a)** that before overload the residual stress and contact stress exist. The residual stress near the crack tip reaches compressive yielding. After overload and at unloading, the compressive yielding zone becomes larger due to the larger reverse yielding. No contact stress exists in the wake of the crack due to crack tip blunting, as shown in **Fig.8(b)**.

When the crack grows further into the overload plastic zone, the contact stress in the wake of the crack becomes larger. Finally the contact stress become the largest in the wake of the crack and the compressive yielding ahead of the crack tip becomes smaller, as shown in **Fig.8(c)(d)(e)**. Here, the ridge of the residual plastic deformation is completely formed and σ_{op} is the highest. Later, a part of crack surface near crack tip are untouched under σ_{min} because of the existence of the ridge. Eventually, the contact stress near the crack tip recovers to the same as before overload, as shown in **Fig.8(f)**. The effect of overload diminishes.

(2) Comparison with test results

Fatigue crack closure behavior is also monitored after the overload application with the specimen C-OLM. The opening stress is determined graphically from $\sigma-\varepsilon$ relation (**Fig.6**). The results are plotted in **Fig.9(a)** against the crack length a for two overload applications. The first overload is applied at a=19.09 mm and the second overload at a=31.49 mm. Before overload, *i.e.* corresponding to the CA load condition, σ_{op} is almost constant. After overload, the value of the opening stress firstly decreases due to crack tip blunting under overload. It gradually increases to the peak value, and finally recovers to that of CA. The two overloads cause the similar tendency of change in σ_{op}.

The change in σ_{op} is calculated under overload

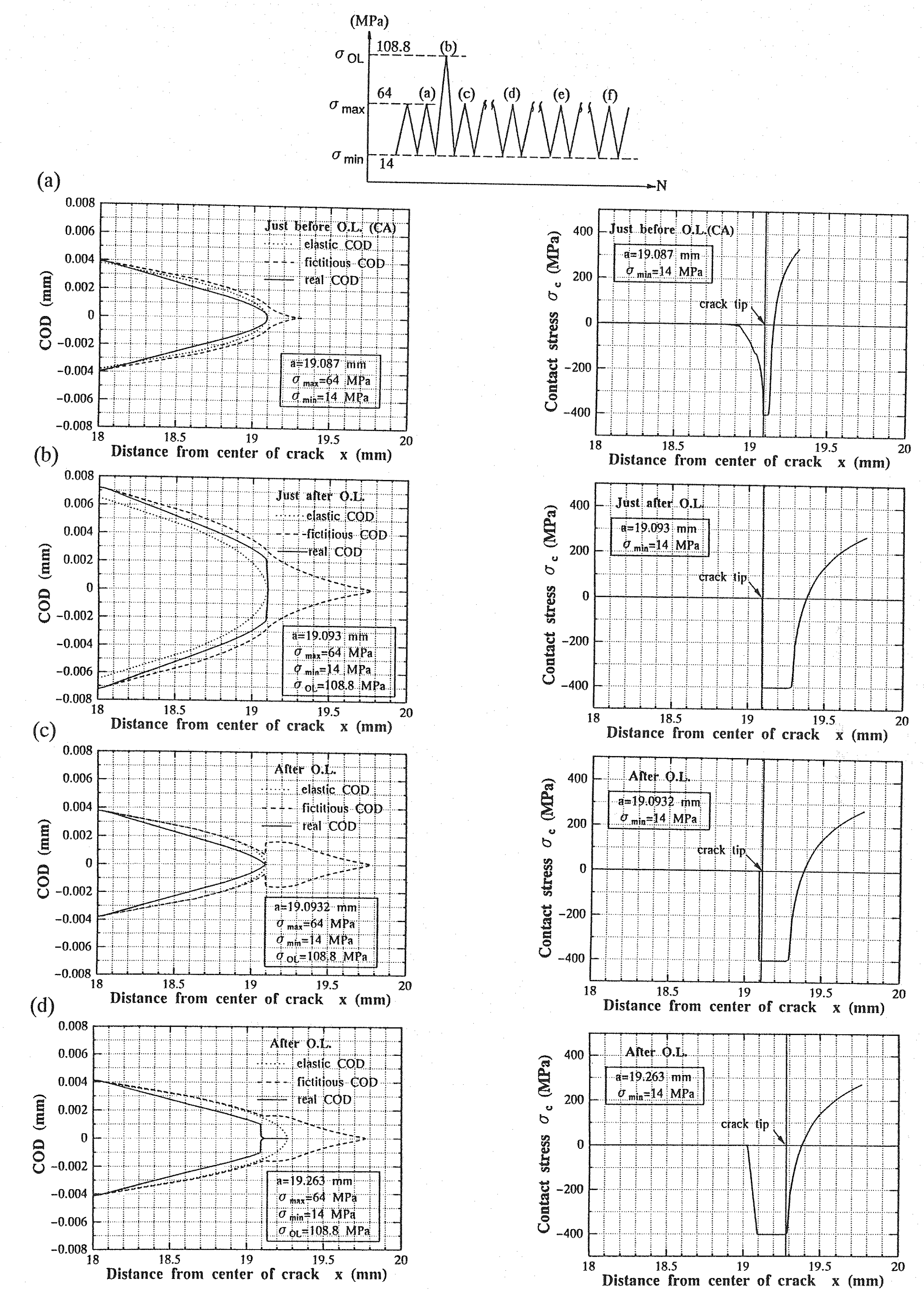

COD at σ_{max} and residual plastic deformation

Contact stress and residual stress at σ_{min}

Fig. 8 Fatigue crack growth behavior under overload condition

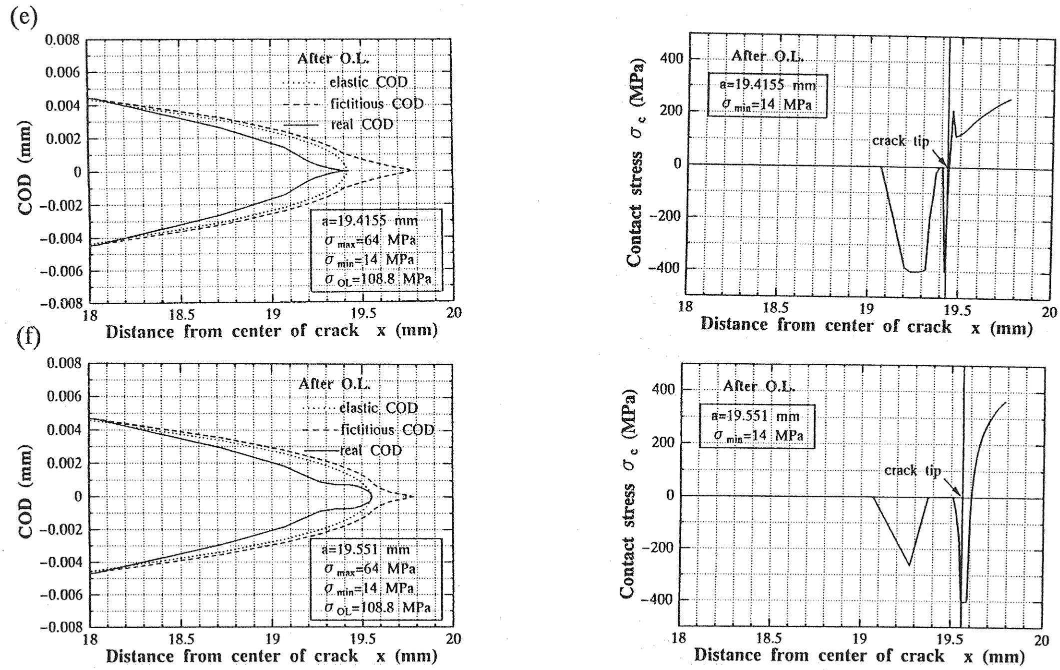

COD at σ_{max} and residual plastic deformation — Contact stress and residual stress at σ_{min}

Fig.8 Fatigue crack growth behavior under overload condition (continued)

condition, and plotted in **Fig.9(a)** with the test result. Both computed and tested opening stress have the same tendency, although the present model gives somewhat larger predicted peak value of σ_{op}.

The fatigue crack growth rates also change in accordance with σ_{op}, as shown in **Fig.9(b)**. The analytical result agrees well with the test result. After overload, the crack growth rates increase firstly, and then decrease to the minimum value, and finally recovers to that of CA. The minimum crack growth rate coincidentally corresponds to the maximum σ_{op}. This change in fatigue crack growth rates corresponds to the fatigue crack growth retardation effect after overloading.

It is noted that for both analytical and test results the overload affected zone is somewhat larger than Dugdale's plastic zone size due to overload, ρ_{OL}. The result is consistent with the conclusion from the previous observation[4].

(3) Fatigue crack propagation life

The analysis is carried out to obtain the relation between fatigue crack length and fatigue crack propagation life under CA and overload conditions. They are compared with the test results, and are shown by the solid lines in **Fig.10**. The analytical results predict well the overall tendency of the test results, although the present model seems to estimate the fatigue crack growth retardation effect due to overload more than the test results for the C-Series specimens.

Analysis is also carried out for other specimens [4]. The overloads are applied three times to each specimen during fatigue crack growth, and the results are listed in **Table 2**. The comparison shows that the analysed fatigue crack propagation lives under overload conditions with constraint factor α=1.68 are generally in good agreement with the test results. The ratio of computed life to the observed life, N_p/N_t, ranges from 0.77 to 1.49, except specimen A-OLH. The mean value of N_p/N_t is 1.08 and the standard deviation is 0.22. The present prediction model is able to predict fatigue life under overload conditions well.

5. ANALYSIS UNDER VARIOUS LOAD SEQUENCES

In order to investigate the load-sequence effect, the analysis is carried out under five load-sequences. They are: (1) CA loading as a reference, (2) single overloading, (3) single underloading, (4) single underload immediately applied after a single overload, and (5) single overload immediately applied after a single underload. The

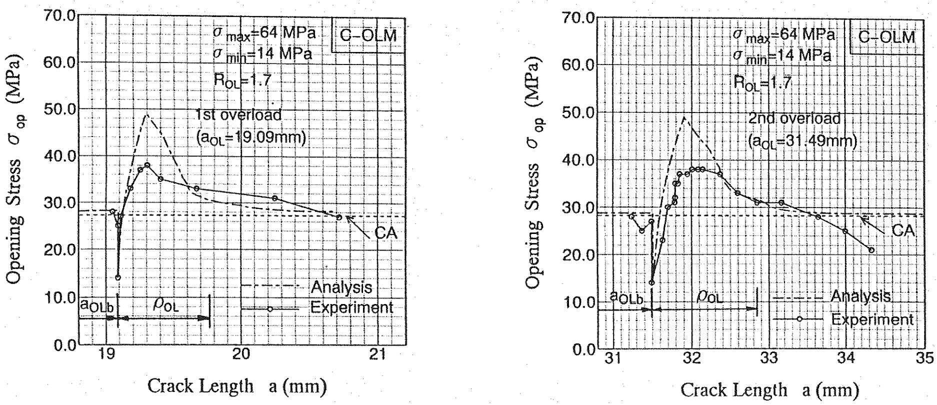

(a) Opening stress

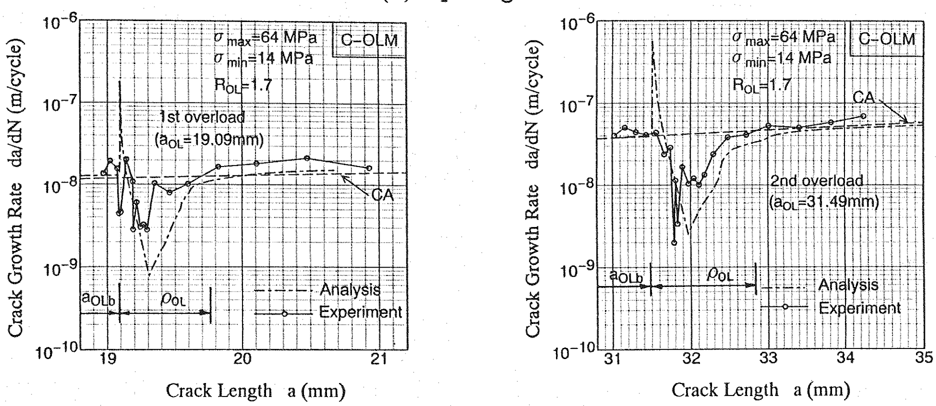

(b) Crack growth rates

Fig. 9 Comparison between analytical and test results under overload condition

Table 2 Comparison of tested and predicted fatigue propagation life under overload conditions (α=1.68)

Specimen No.	a_0 (mm)	N_0 ($\times 10^3$ cycles)	a_f (mm)	N_f ($\times 10^3$ cycles)	N_t $=N_f$-N_0	N_p (**Eq.(9)**)	N_p/N_t
A-CA	7.87	715	53.52	1525	810	935	1.15
A-OLH	8.58	949	42.49	1978	1029	2504	2.43
A-OLM	8.87	1243	43.75	2310	1067	1112	1.04
A-OLL	8.88	815	54.48	1584	769	875	1.14
B-CA	8.80	708	41.90	1402	694	559	0.81
B-OLL	7.94	637	47.13	1418	781	809	1.04
B-OLLL	8.51	710	39.84	1505	795	614	0.77
C-CA	10.11	9761	50.25	12015	2254	2131	0.95
C-OLH	10.04	2067	50.36	4540	2473	3693	1.49
C-OLM	12.10	1696	43.08	3122	1426	1862	1.31

* a_0, a_f - initial and final crack length for crack growth rate measurement
** N_0, N_f - number of cycles with crack length a_0, a_f
*** N_t, N_p - tested and predicted fatigue propagation life

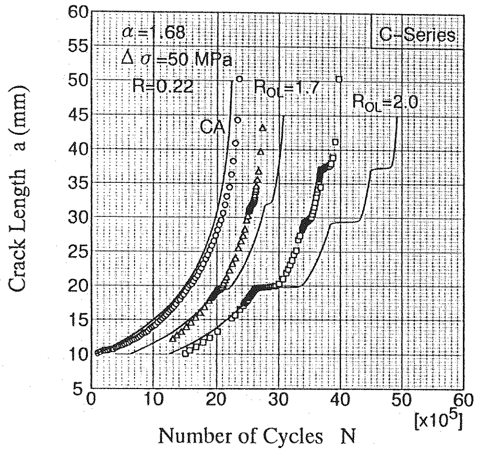

Fig. 10 Fatigue crack propagation life under overload condition

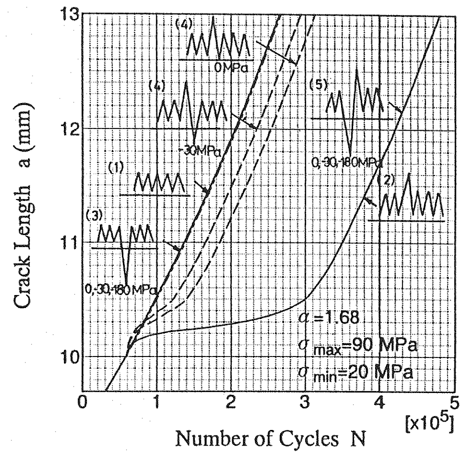

Fig. 11 Fatigue crack propagation life under various load sequences

σ_{max} and σ_{min} of CA are 90 MPa and 20 MPa, respectively. The overload is 153 MPa ($R_{OL} = 1.7$). The underloads are chosen as 0, -30 and -180 MPa ($R_{UL} = 0, -0.33$, and -2.0).

The analytical result, as shown in **Fig.11**, indicates that sequence (2) and sequence (5) cause almost the same retardation effect on fatigue crack growth rates. The underload applied after overload, *i.e.* sequence (4), significantly reduces the overload retardation effect, as shown by dashed lines in **Fig.11**. The underload tends to eliminate the retardation effect of overload, because the underload causes more reverse plastic deformation than the normal unloading. The lower level of the underload after overload makes the overload retardation effect even less. If the underload is low enough, the overload retardation effect may be eliminated completely.

For sequence (3), the underload causes little effect on the opening stress, and therefore little effect on fatigue crack propagation life. The results at the underload levels of 0, -30 and -180 MPa show little difference, and the prediction gives almost the same result as without the underload. Therefore, the effect of an underload applied before CA loading or overloading can be neglected.

6. CONCLUSIONS

In the present study, fatigue crack closure test and analysis are carried out with the center-cracked tension specimens of structural steel JIS SM520B. The crack closure, which is caused by the remaining plastic deformations in the wake of an advancing crack, causes the load interaction effects on the fatigue crack growth rates. A fatigue crack growth prediction model based on crack closure concept is applied to compute the effective stress intensity factor range. The high-low load sequence effect is emphasized to verify the present model. The analytical results are compared with test results under CA loading and overloading conditions. The analysis of fatigue crack propagation life is also carried out under various load conditions to investigate load interaction effect. The findings are summarized as follows:

1. Stress ratio has large effect on the opening stress when $0 \leq R < 0.7$. Opening stress is almost equal to the minimum stress when $R \geq 0.7$ due to the permanent crack opening.
2. Effective stress intensity factor, ΔK_{eff}, is correlated with crack growth rates under CA loading. The constants m=3.257 and C=9.321×10^{-12} are obtained for the structural steel JIS SM520B.
3. Under overload condition, the opening stress varies when crack grows through the plastic zone due to overload. The overload affected zone size is somewhat larger than the Dugdale's plastic zone size. The peak value of the opening stress, and hence the valley value of crack growth rates, result from the ridge of plastic deformation due to overload. The analytical results are in good agreement with the test results.
4. The present model can predict well the fatigue crack propagation life with the consideration of load interaction effect. For three periodic overload conditions, the ratio of the predicted life to the observed life ranges from 0.77 to 1.49. The mean value is 1.08.

5. The load-sequence effect is investigated for various load sequences. The high-low load sequence causes retardation effect. The underload applied after overload eliminates the retardation effect of overload. The low-high sequence has very little acceleration effect, and it can be neglected.

REFERENCES

1) Suzuki, N., Takeda, H., Ohta, A. and Ohuchida, H. : Evaluation of fatigue crack propagation properties under random loading avoiding crack closure, *Fatigue Fract. Engng. Mater. Struct.*, Vol.14, No.8, pp.815-821, 1991.
2) Yamada, K. and Cheng, X. H. : Fatigue life analysis on welded joints under various spectrum loadings, *Journal of Structural Engineering*, Vol.39A, pp.947-957, March, 1993.
3) Johnson, W. S. : Multi-parameter yield zone model for predicting spectrum crack growth, *Methods and Models for Predicting Fatigue Crack Growth under Random Loading*, ASTM STP 748, pp.85-102, 1981.
4) Cheng, X. H., Okuhara, Y., Yamada, K. and Kondo, A. : Fatigue crack growth rate measurement of structural steel under overload conditions, *Proc. of JSCE, Structural Eng./Earthquake Eng.*, Vol.11, No.1, pp.45-52, April, 1994.
5) Zhang, X., Chan, A. S. L. and Davies, G. A. O. : Numerical simulation of fatigue crack growth under complex loading sequences, *Engineering Fracture Mechanics*, Vol.42, No.2, pp.305-321, 1992.
6) Booth, G. S. and Maddox, S. J. : Correlation of fatigue crack growth data obtained at different stress ratios, *Mechanics of Fatigue Crack Closure*, ASTM STP 982, pp.516-527, 1988.
7) Abtahi, A., Albrecht, P. and Irwin, G. R. : Fatigue of periodically overloaded stiffener detail, *Proc. of ASCE, Journal of the Structural Division*, Vol.102, No. ST11, pp.2103-2109, Nov., 1976.
8) Albrecht, P. and Yamada, K. : Simulation of service fatigue loads for short-span highway bridges, *Service Fatigue Loads Monitoring, Simulation, and Analysis*, ASTM STP 671, pp.255-277, 1979.
9) Melhem, H. G. and Klippstein, K. H. : A study on variable amplitude load fatigue: Work-in-Progress, Research Report No. ST-6, Department of Civil Engineering, University of Pittsburgh, January, 1990.
10) Wheeler, O. E. : Spectrum loading and crack growth, *Trans. of ASCE, Journal of Basic Engineering*, Vol.94, No.1, pp.181-186, 1972.
11) Elber, W. : The significance of fatigue crack closure, *Damage Tolerance in Aircraft Structures*, ASTM STP 486, pp.230-242, 1971.
12) Newman, J. C., Jr. : A finite-element analysis of fatigue crack closure, *Mechanics of Crack Growth*, ASTM STP 590, pp.281-301, 1976.
13) Chermahini, R. G., Shivakumar, K. N. and Newman, J. C., Jr. : Three-dimensional finite-element simulation of fatigue crack growth and closure, *Mechanics of Fatigue Crack Closure*, ASTM STP 982, pp.398-413, 1988.
14) Newman, J. C., Jr. : A crack-closure model for predicting fatigue crack growth under aircraft spectrum loading, *Methods and Models for Predicting Fatigue Crack Growth under Random Loading*, ASTM STP 748, pp.53-84, 1981.
15) *de* Koning, A. U. and Liefting, G. : Analysis of crack opening behavior by application of a discretized strip yield model, *Mechanics of Fatigue Crack Closure*, ASTM STP 982, pp.437-458, 1988.
16) Wang, G. S. and Blom, A. F. : A strip model for fatigue crack growth predictions under general load condition, *Engineering Fracture Mechanics*, Vol.40, No.3, pp.507-533, 1991.
17) Liaw, P. K. : Overview of crack closure at near-threshold fatigue crack growth levels, *Mechanics of Fatigue Crack Closure*, ASTM STP982, pp.62-92, 1988.
18) Dugdale, D. S. : Yielding of steel sheets containing slits, *Journal of the Mechanics and Physics of Solids*, Vol.8, pp.100-104, 1961.
19) National Research Institute for Metals : Fatigue crack propagation properties in arc-welded butt-joints of high strength steels for welded structure, *NRIM Fatigue Data Sheet Technical Document*, No.3, p.37, 1984 (in Japanese).
20) Yamada, K. : Fatigue crack growth rates of structural steels under constant and variable amplitude block loading, *Proc. of JSCE, Structural Eng./Earthquake Eng.*, Vol.2, No.2, pp.25-33, October, 1985.
21) Japanese Society of Steel Construction : Fatigue Design Recommendations, Gihoudou, 1993 (in Japanese).
22) Hertzberg, R. W. : Deformation and fracture mechanics of engineering material, John Wiley & Sons, Inc., 1976.
23) Nishida, M. : Stress concentration, Morikita Publication, 1973 (in Japanese).

(Received July 20, 1994)